J|A|C|S ARTICLES

Published on Web 09/14/2009

Predicted Trends of Core−Shell Preferences for 132 Late Transition-Metal Binary-Alloy Nanoparticles

Lin-Lin Wang and Duane D. Johnson*

Department of Materials Science and Engineering, and Frederick Seitz Materials Research Laboratory, University of Illinois, 1304 West Green Street, Urbana Illinois 61801

Received April 22, 2009; E-mail: duanej@illinois.edu

Abstract: Transition-metal alloyed nanoparticles with core−shell features (shell enrichment by one of the metals) are becoming ubiquitous, from (electro-)catalysis to biomedical applications, due to their size control, performance, biocompatibility, and cost. We investigate 132 binary-alloyed nanoparticle systems (groups 8 to 11 in the Periodic Table) using density functional theory (DFT) and systematically explore their segregation energies to determine core−shell preferences. We find that core−shell preferences are generally described by two independent factors: (1) *cohesive energy* (related to vapor pressure) and (2) *atomic size* (quantified by the Wigner−Seitz radius), and the interplay between them. These independent factors are shown to provide general trends for the surface segregation preference for atoms in nanoparticles, as well as semi-infinite surfaces, and give a simple correlation (a "design map") for the alloying and catalytic behavior. Finally, we provide a universal description of core−shell preference via tight-binding theory (band-energy differences) that (i) quantitatively reproduces the DFT segregation energies and (ii) confirms the electronic origins and correlations for core−shell behavior.

Introduction

Nanoscale transition-metal (TM) nanoparticles exhibit enormous complexity,[1] with their structure and properties intimately connected and, at times, varying dramatically.[2,3] Late TM alloyed nanoparticles with core−shell features have been shown to improve catalytic, magnetic, optical, and biomedical properties needed in a wide range of applications. It is of great importance to understand the driving force and physical quantities that determine core−shell preferences, i.e., which metal goes into the core and which into the shell, in order to design core−shell nanoparticles with desired properties.

Despite the large and growing interest in core−shell nanoparticles, the understanding of core−shell preference is based largely on observation of a limited number of synthesized binaries in experiments and a few core−shell combinations focused in individual theoretical studies (see recent review[4]). The picture emerging thus far from these studies is that there are a few factors that determine core−shell preferences. Factors most often mentioned are cohesive energy, surface energy, atomic radii, and electronegativity.[4] For example, metals with larger cohesive and/or surface energies should tend to be in the core to achieve the greatest binding among the constituents. Alternatively, metals with smaller atomic radii would tend to favor the core to relieve compressive strain.

However, such understanding is limited because a critical understanding of the interplay among these factors is still lacking, and key questions remain unanswered. For example, are these factors independent, or, if not, then what are the primary and secondary factors controlling core−shell behavior? Do these factors act cooperatively or competitively? And more importantly, are there general trends determined synergistically by the independent factors that govern core−shell preference? Finding the general trends and answers to the above questions requires using the same theoretical methods to study a range of core−shell combinations for nanoparticles and then compiling a database.

On a closely related front, databases of the surface segregation energy (SE) of a single impurity on semi-infinite close-packed fcc(111)[5] and open fcc(100)[6] surfaces have been calculated from density functional theory[7,8] (DFT). Just as the segregation energy provides a quantitative assessment of segregation behavior in bulk alloys (i.e., miscibility[9]) or in semi-infinite bulk alloys (i.e., surface segregation[5,6]), so too does it permit assessment of core−shell preference in nanoparticles. Although in general the surface segregation energy depends on the composition and temperature of the bulk alloy (and size for nanoparticle), these data for a single impurity (i.e., in the diluted limit) can be used as an estimate of surface segregation energies for bulk alloy, and also for nanoparticles of large sizes to give core−shell preference. However, as the size of nanoparticles decreases (i.e., 1 nm and a few hundred atoms), the surface segregation energy can change due to a higher surface-to-volume ratio, larger

(1) Frenkel, A. I.; Yang, J. C.; Johnson, D. D.; Nuzzo, R. G. In *Encyclopedia of Complexity and Systems Science*; Meyers, R. A., Ed.; Springer: Heidelberg, Germany, in print.
(2) Baletto, F.; Ferrando, R. *Rev. Mod. Phys.* **2005**, *77*, 371–423.
(3) Wang, L. L.; Johnson, D. D. *Phys. Rev. B* **2007**, *75*, 235405.
(4) Ferrando, R.; Jellinek, J.; Johnston, R. L. *Chem. Rev.* **2008**, *108*, 845–910.
(5) Ruban, A. V.; Skriver, H. L.; Norskov, J. K. *Phys. Rev. B* **1999**, *59*, 15990–16000.
(6) Nilekar, A. U.; Ruban, A. V.; Mavrikakis, M. *Surf. Sci.* **2009**, *603*, 91–96.
(7) Hohenberg, P.; Kohn, W. *Phys. Rev. B* **1964**, *136*, B864–B871.
(8) Kohn, W.; Sham, L. J. *Phys. Rev.* **1965**, *140*, A1133–A1138.
(9) Zarkevich, N. A.; Tan, T. L.; Johnson, D. D. *Phys. Rev. B* **2007**, *75*, 104203.

change in coordination number, more relaxation in volume, and stronger magnetic effect than semi-infinite surfaces. Thus, it demands a similar database for small nanoparticles.

To provide answers to the questions concerning the interplay among the factors that determine core−shell preference and find the general trends to benefit understanding and design of alloyed nanoparticle properties, we herein calculate the surface segregation energies of a single impurity in a 55-atom cuboctahedron cluster for 132 binary alloyed systems composed of twelve late-TMs using DFT. Then, by correlating the segregation energies with basic properties (confirmed within a tight-binding model), we show that core−shell preferences are described largely by the interplay between two independent factors: (1) *cohesive energy* and (2) *atomic size* (quantified by the Wigner−Seitz (WS) radius), leading to general trends. Apart from identifying simple correlations and resulting rules that predict core−shell preference, we also provide a universal description of core−shell preferences via tight-binding (TB) theory, using band-energy differences[10−12] via the moment theorem,[12−14] that (i) quantitatively reproduces the SE from DFT and (ii) confirms the origin of core−shell behavior.

In general, binary bulk alloys can have configurations that span from segregation (immiscible) to total mixing (a homogeneous random alloy) as well as ordering at some specific compositions (e.g., line compounds). By creating surfaces, even random alloys will have one component enrich the surface layers, which is surface segregation. At the nanoscale, due to the high surface-to-volume ratio, surface segregation becomes more and more dominant. Also due to the possibility of greater volume relaxation, alloys that may exhibit segregation in bulk may mix in the nanoparticle scale. For these reasons, core−shell is the most frequently observed configuration in alloyed nanoparticles and the first question that is addressed. By assigning a *core−shell preference*, we do not mean a perfect core−shell configuration; rather, we mean the relative enrichment of a shell by one metal over another. For each binary combination, a thorough search for groundstate structure and configuration at different composition should be done to study the specific configuration,[15−18] as shown by a recent finding of a pure-shell, mixed-core structure.[19] Here, we do not intend to oversimplify the problem, but to identify general trends through calculations that already reflect some underlying principles.

Computational Details

To determine SE for a general nanoparticle composition and structure, we consider the energy difference (after full atomic relaxations) of

$$\Delta E_{(A)B} = E_{(A_{m-1}B)AB_{n-1}} - E_{(A_m)B_n} \equiv \Delta^{c_0}_{AB} \quad (1)$$

between a nanoparticle with m A atoms in the core (denoted within parentheses) and n B atoms in the shell and one with two atoms exchanged between the core and shell, where $c_0 = m/(m + n)$ is the composition of A. The SE defined in eq 1 is valid regardless of the core and shell size or the particular morphology of the particle. For $m = 1$ and general systems size $(m + n)$, the SE is also known as the "impurity formation energy".

In particular, Figure 1(a) shows a 55-atom cuboctahedron cluster ($m = 1$ and $n = 54$) that we use to calculate SE before the exchange of core−shell (or impurity-host) atoms and after (Figure 1(b)). Although the definition is quite general, the magnitude of SE depends on which site is chosen to be the segregated site (given that the core site is the central site of the cluster). Here, we choose one of the corner sites, as shown in Figure 1(b), which is part of both (111) and (100) facets. This offers a new perspective compared to the surface segregation calculations on semi-infinite (111) and (100) surfaces. Other segregated sites on the shell, such as the central site in the (111) and (100) facets, are also possible. The dependence of SE on the surface site is worthy of study, but involves many more of the CPU-intensive calculations over several surface configurations, which remains for future study.

Of course, we understand that this 55-atom cuboctahedron particle is not necessarily the lowest-energy structure at the given size and composition,[15,16] but it generically describes the driving force for core−shell preference because the segregation energy is the energy difference and some cancellation effect should be expected. For example, as confirmation, a recent study[17] using 38-atom clusters of Pd−Pt, Ag−Au, Pd−Au, and Ag−Pt in structures other than truncated octahedral found the same core−shell preferences as in the truncated octahedron. Recently, functional properties of magnetic nanoparticles of FePt and CoPt were investigated versus size (55 to 561 atoms) and morphology;[20] the same core−shell preferences were found for these larger nanoparticles as those found in our results on the 55-atom cluster. Given the similar general trends for core−shell preference found from a 55-atom cluster to semi-infinite surfaces and the success of the same analysis based on universal tight-binding model (see below), we believe that the trends we found in the current study are quite general.

DFT results were obtained using the Vienna Atomic Simulation Package[21,22] (VASP) within a generalized gradient approximation to the exchange-correlation functional (GGA given by PW91[23]), a projected augmented wave[24] (PAW) basis, and the default plane-wave kinetic energy cutoffs.[25] Particles were simulated in a periodic cubic cell with 20 Å sides, avoiding interactions among a particle's periodic images with about 12 Å vacuum. Using Γ k-point, i.e., Γ = (000), the energies were converged to 1 m*e*V/atom and ionic relaxations were allowed until the absolute value of force on each atom were below 0.02 *e*V/Å. We confirmed that these results are converged with respect to k-points mesh and vacuum size.

Segregation Energies for 132 Alloyed 55-Atom Clusters. In Table 1, DFT-PW91 calculated segregation energies in eV for 132 binary alloy nanoparticles are listed. Clearly, a positive $\Delta E_{(A)B}$ indicates a core−shell structure that prefers A in the core and B in the shell; the larger the magnitude the greater the tendency. In contrast, a negative $\Delta E_{(A)B}$ indicates the opposite preference: A in the shell and B in the core. For example, for Pt-core and Ag-shell configuration, the positive SE (+0.84 eV) indicates that the present

(10) Pettifor, D. G. *Commun. Phys.* **1976**, *1*, 141.
(11) Mackintosh, A. R.; Andersen, O. K. In *Electrons at the Fermi Surfaces*; Springford, M., Ed.: Cambridge, 1980.
(12) Ducastelle, F. *Order and Phase Stability in Alloys*; North-Holland, Elsevier Sceince Publishers B. V.: Amsterdam, The Netherlands, 1991.
(13) Cyrot-Lackmann, F. *J. Phys. Chem. Solids* **1968**, *29*, 1235–1243.
(14) Ducastelle, F.; Cyrot-Lackmann, F. *J. Phys. Chem. Solids* **1970**, *31*, 1295–1306.
(15) Rossi, G.; Rapallo, A.; Mottet, C.; Fortunelli, A.; Baletto, F.; Ferrando, R. *Phys. Rev. Lett.* **2004**, *93*, 105503.
(16) Ferrando, R.; Fortunelli, A.; Rossi, G. *Phys. Rev. B* **2005**, *72*, 085449.
(17) Paz-Borbon, L. O.; Johnston, R. L.; Barcaro, G.; Fortunelli, A. *J. Chem. Phys.* **2008**, *128*, 134517.
(18) Wang, G.; Van Hove, M. A.; Ross, P. N.; Baskes, M. I. *Prog. Surf. Sci.* **2005**, *79*, 28–45.
(19) Calvo, F.; Cottancin, E.; Broyer, M. *Physical Review B (Condensed Matter and Materials Physics)* **2008**, *77*, 121406.
(20) Gruner, M. E.; Entel, P. *J. Phys.: Condens. Matter* **2009**, *21*, -.
(21) Kresse, G.; Furthmüller, J. *Comput. Mater. Sci.* **1996**, *6*, 15–50.
(22) Kresse, G.; Furthmüller, J. *Physical Review B: Condensed Matter* **1996**, *54*, 11169–11186.
(23) Perdew, J. P.; Wang, Y. *Phys. Rev. B* **1992**, *45*, 13244–13249.
(24) Blöchl, P. E. *Phys. Rev. B* **1994**, *50*, 17953–17979.
(25) *Kinetic energy cutoff in eV, Au 229.9, Ag 249.8, Cu 273.2, Pt 230.3, Pd 250.9, Ni 269.6, Ir 210.9, Rh 229.0, Co 268.0, Os 228.0, Ru 213.3 and Fe 267.9.*

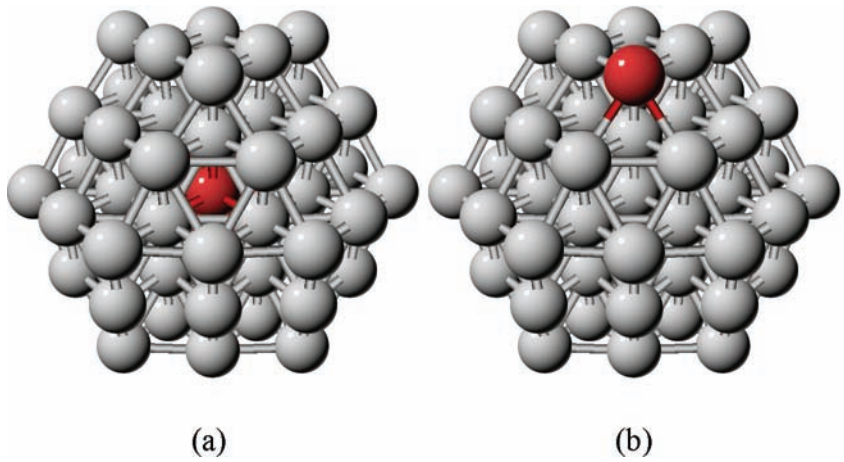

Figure 1. The cuboctahedral 55-atom clusters used in determining segregation energies (defined in text). Red (gray) spheres stand for A (B) atoms.

Table 1. DFT-PW91 Calculated Segregation Energies in eV for 55-Atom Binary Alloy Nanoparticles[a]

	Au	Ag	Cu	Pt	Pd	Ni	Ir	Rh	Co	Os	Ru	Fe
Au	0	−0.06	−0.67	−1.77	−0.67	−2.02	−3.36	−2.22	−2.05	−2.93	−1.90	−4.70
Ag	0.07	0	−0.77	−1.99	−0.82	−2.29	−3.54	−2.41	−2.15	−3.03	−1.96	−5.20
Cu	0.47	0.08	0	−0.24	0.26	−0.81	−1.93	−0.99	−0.71	−1.61	−0.72	−2.58
Pt	1.01	0.84	0.41	0	0.51	−0.61	−1.37	−0.70	−0.95	−1.45	−0.66	−2.71
Pd	0.89	0.70	0.13	−0.44	0	−1.09	−1.71	−1.13	−1.29	−1.67	−0.84	−3.26
Ni	0.95	0.67	0.72	0.42	0.46	0	−0.67	−0.17	−0.20	−0.48	0.04	−2.02
Ir	1.48	1.51	1.22	1.48	1.34	0.33	0	0.23	−0.04	−0.40	0.07	−1.97
Rh	1.28	1.33	0.90	0.75	0.79	−0.23	−0.36	0	−0.53	−0.66	−0.12	−2.87
Co	0.52	0.36	0.73	0.94	0.75	0.15	0.04	0.16	0	0.13	0.11	−2.24
Os	1.54	1.68	1.71	2.52	1.95	0.92	0.65	0.54	0.72	0	0.14	−0.34
Ru	1.43	1.46	1.30	1.76	1.14	0.19	0.38	0.42	0.07	−0.18	0	−2.24
Fe	0.77	0.60	1.83	0.82	0.74	−0.10	0.00	−0.02	0.07	−0.08	−0.29	0

[a] The row (column) is for core (shell) or impurity (host) in the nanoparticle.

configuration is preferred, whereas a negative SE (−0.61 eV) for Pt-core and Ni-shell configuration means that a Pt-shell and Ni-core is preferred.

For the complementary case, the segregation preference of B as an impurity in an A majority nanoparticle also correlates with the segregation and core−shell preferences. For example, the Ag-core and Pt-shell configuration has a negative SE of −1.99 eV, which means that the Ag-shell and Pt-core is preferred—the same preference as noted already for the positive SE for Pt-core and Ag-shell configuration. Another example is that with an Ag-core and Au-shell preference; although SE from a semi-infinite surface predicts it the other way around, our SE for nanoparticles agrees with more detailed DFT calculations, even with structures other than truncated octahedron.[17]

For a few combinations (10 pairs out of 66 pairs of alloys), the same preference does not always hold at the two complementary dilute limits, such as Cu−Pd. The positive SE (+0.26 eV) for Cu-core impurity and Pd-shell indicates a preference for Cu-core and Pd-shell in the dilute-Cu limit, and, in contrast, the positive SE (+0.13 eV) for Pd-core impurity and Cu-shell indicates that a Pd-core and Cu-shell is preferred in the dilute-Pd limit. Both core−shell features have been observed in experiments depending on composition and temperaure.[26] Experimentally Cu-rich surfaces at low-Cu content are not observed, and this agrees with our SE results, indicating that the core−shell preference indeed depends on the composition. These complex cases should be treated carefully and subjected to further study. Here, we want to emphasize that the majority of core−shell preferences obey specific general trends (our focus here) as discussed below, none of which have been previously discussed. In addition, we will identify the two independent physical properties that determine such trends, as well as their underlying electronic origins.

Predicted Correlations and Trends in Core−Shell Preference. Although there is general agreement that the core−shell preference is affected by atomic radius, cohesive energy, surface energy, and so forth, as summarized in ref 4, very little discussion has been given to the interplay among these factors. A quick alignment in *d* series, as done in the case of semi-infinite surfaces,[5,6] does not reveal an overall correlation or the key factors dictating core−shell behavior. It will be of more benefit to engage in a type of principal component analysis[27] to identify the independent factors that are dominating and show general trends, such as a highly correlated shell-to-core sequence to tell if a metal is more likely to be in the shell when alloyed with other metals, similar to that frequently done for metal reduction reactions in electrochemistry with the sequence of electrode potential. As shown in Table 1, we chose the metal sequence to make the upper (lower) half matrix almost negative (positive). For ease of visualization, the data from Table 1 is shown color-coded in Figure 2. Clearly, Figure 2 shows the existence of a strong correlation of SE and alloying core−shell preference when atoms are collected by groups (aligned by cohesive energy) and ordered according from 5d, 4d, to 3d (aligned by atomic size), revealing the two principal factors for segregation and core−shell preference. Only in this particular sequence does the metal on the left (top) almost always prefer the shell when alloyed with a metal on the right (bottom).

To find the independent factors, the most strongly correlated ones should be identified first. We plot those factors in Figure 3 for the entire TM series. As shown in Figure 3(a), the highest cohesive

(26) Sun, K.; Liu, J.; Nag, N. K.; Browning, N. D. *J. Phys. Chem. B* **2002**, *106*, 12239–12246.

(27) Wold, S.; Esbensen, K.; Geladi, P. *Chemometrics and Intelligent Laboratory Systems* **1987**, *2*, 37–52.

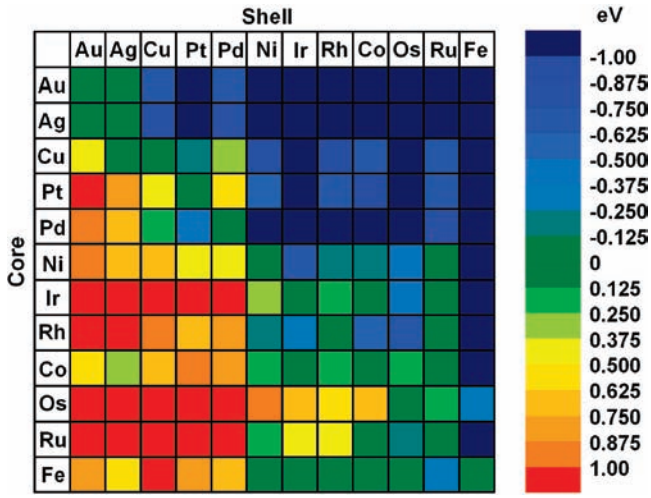

Figure 2. Color-coded matrix of DFT-PW91 segregation energies for impurity in 55-atom nanoparticle composed of 12 late-transition metals (132 binaries).

energies[28] lies in the middle of TM series, as expected from band-filling arguments (bonding states are filled while antibonding states are empty). The drop in 3d cohesive energy is due to magnetism. Generally, within a group, 5d has larger cohesive energy than 4d, which is in turn higher than 3d, except near the end of the TM series. From the RCA gas tables,[29] the temperature for a given vapor pressure (Figure 3(c)) are included because, from free energy arguments, it is intuitive to think that, between alloyed metals, the metal with the lowest temperature to reach a given vapor pressure will segregate to the surface of the other metal—a valid rule of thumb, in fact, for bulk, semi-infinite bulk and nanoparticle alloys. Figure 3(c) shows that vapor pressure also correlates directly with cohesive energy, since sublimation energy correlates closely with melting temperature or cohesive energy. Surface energies[30] (Figure 3(d)) follow the same trend as bulk cohesive energies (Figure 3(a)), understandable from simple bond-counting arguments. Hence, only cohesive energy is the independent energy metric.

The atomic size in terms of WS radius[28] (Figure 3(b)) gives a different trend from the cohesive energy. Among groups, going from the late to middle TM series, the cohesive energy increases while the WS radius decreases, with 5d larger than 4d and 3d; but the difference between 4d and 5d is very small. The atomic size affects core−shell preference in that the TM with smaller WS radius tends to be in the core to relieve strain. Notably, the atomic radius, defined as half of the first nearest-neighbor distance, was used in the recent review.[4] However, for TMs, the WS radius is the more relevant parameter, as it directly determines the atomic size,[31] d-bandwidth,[32] and energy, as is well-known from tight-binding theory.

From these trends, only if the atoms are aligned *first* by group going from late to middle TM (smallest cohesive energy to largest) and then *second* by size within a group from 5d, 4d to 3d (largest to smallest WS radius), as shown in Figure 2, does the SE appear in the most correlated pattern. To contrast, we have aligned the SE data according to either only increasing cohesive energy (Figure 4(a)) or decreasing WS radius (Figure 4(b)). It is visually apparent that, unlike when ordered according to both cohesive energy between groups and WS radius within a group, there are only some correlations found/recovered. For example, Pt and Fe are clear exceptions when correlated by only cohesive energy (Figure 4(a)), and Cu and Fe have low correlations with other metals when aligned by only WS radius (Figure 4(b)).

For a binary nanoparticle formed by metals from different groups, the two factors of cohesive energy and WS radius act cooperatively, as metal, going from late to middle of TM series, of both a larger cohesive energy and a smaller radius prefers to be in the core region. In contrast, for nanoparticles formed by metals within a group, going from 5d to 3d, the cohesive energy gets smaller, but the WS radius becomes smaller, too. Now the two factors act competitively. In such cases, WS radius dominates most of the time; some exceptions are the ones around the diagonal for nanoparticles of 4d and 5d within the same group. For these exceptions, the 5d and 4d from the same group have almost the same WS radius, and, hence, the cohesive energy is dominant again, such as, Pt−Pd, Ir−Rh, and Os−Ru. These general trends/correlations and simple rules work quite well, as indicated in Figure 2. Moreover, similar analysis can also be applied to reveal the core−shell preference for multicomponent nanoparticles.

Core−Shell Preference from Nanoparticles to Bulk. As noted, SE provides a quantitative assessment of generic segregation behavior. The governing factors of cohesive energy and WS radius controlling segregation behavior are not restricted to nanoparticles. In Figure 5, we show the DFT surface-segregation energies for semi-infinite alloys[5] using the same color-coding and ordering as found in Figure 2, i.e., cohesive energy between groups and WS radius within a group. Again, the general segregation trend is remarkably reproduced when organized using these two key factors, regardless of whether the surface is close-packed (111) or less close-packed (100). The major distinction between nanoparticles and semi-infinite surfaces is that the nanoparticle SE is larger than for surfaces[5] because of larger change in coordination number, more relaxation in volume and stronger magnetization.

Design Maps for Core−Shell Nanoparticles. Figures 2 (55-atom nanoparticles) and 5 (semi-infinite surfaces) each constitute a "design map" to predict the surface enrichment of an alloying element. (This can, of course, be done for multicomponent nanoparticles, or for defects, such as vacancies, which can change catalytic reactivity.) Hence, many useful predictions for nanoparticles can be made from results in Figure 2. In fuel cells, Pt-based nanoparticles are desired to improve electrocatalysis at the cathode and anode. With the exception of Au, Ag, and Pd, Figure 2 shows that Pt prefers to be in shell when alloyed with other late TMs, particularly 3d TMs, even though their cohesive energies are much smaller than Pt. Hence, Pt-based binary nanoparticles can form a shell of catalytically active Pt.[18,33,34] Also, Fe has the highest core preference when alloyed with late TMs. Given its abundance, hence low cost, Fe-based core−shell nanoparticles are good candidates for use in a range of applications, such as lower-cost, Se-decorated Fe-core/Ru-shell for oxygen reduction reactions, rather than the Se-decorated large Ru particles.[35] Fe−Au would be good for fluorescence biomarkers, rather than pure Au particles.[36]

Of course, ligand-modified, core−shell preferences should be studied to gain more insight in functionalizing core−shell nanoparticles. For example, one technological necessity would be to determine how these "design maps" can be amended to account for adsorption of organics, which may alter (or even reverse) the surface-enrichment preferences for nanoparticles, as seen for bulk-like surfaces,[37] or change their morphology as often observed.[38]

(28) Kittel, C. *Introduction to Solid State Physics*; 7 ed.; Wiley: New York, 1996.
(29) Honig, R. E.; Kramer, D. A. *RCA Review* **1969**, *30*, 285.
(30) de Boer, F. R.; Boom, R.; Mattens, W. C. M.; Miedema, A. R.; Niessen, A. K. *Cohesion in Metals* Amsterdam, North-Holland, 1988.
(31) Pinski, F. J.; Ginatempo, B.; Johnson, D. D.; Staunton, J. B.; Stocks, G. M.; Gyorffy, B. L. *Phys. Rev. Lett.* **1991**, *66*, 766–769.
(32) Harrison, W. A. *Electronic Structure and the Properties of Solids*; W. H. Freeman and Company: San Francisco, USA, 1980.
(33) Stamenkovic, V. R.; Fowler, B.; Mun, B. S.; Wang, G. F.; Ross, P. N.; Lucas, C. A.; Markovic, N. M. *Science* **2007**, *315*, 493–497.
(34) Ma, Y.; Balbuena, P. B. *Surf. Sci.* **2008**, *602*, 107–113.
(35) Cao, D. X.; Wieckowski, A.; Inukai, J.; Alonso-Vante, N. *J. Electrochem. Soc.* **2006**, *153*, A869–A874.
(36) Elghanian, R.; Storhoff, J. J.; Mucic, R. C.; Letsinger, R. L.; Mirkin, C. A. *Science* **1997**, *277*, 1078–1081.
(37) Han, B. C.; Van der Ven, A.; Ceder, G.; Hwang, B. J. *Phys. Rev. B* **2005**, *72*, 205409.

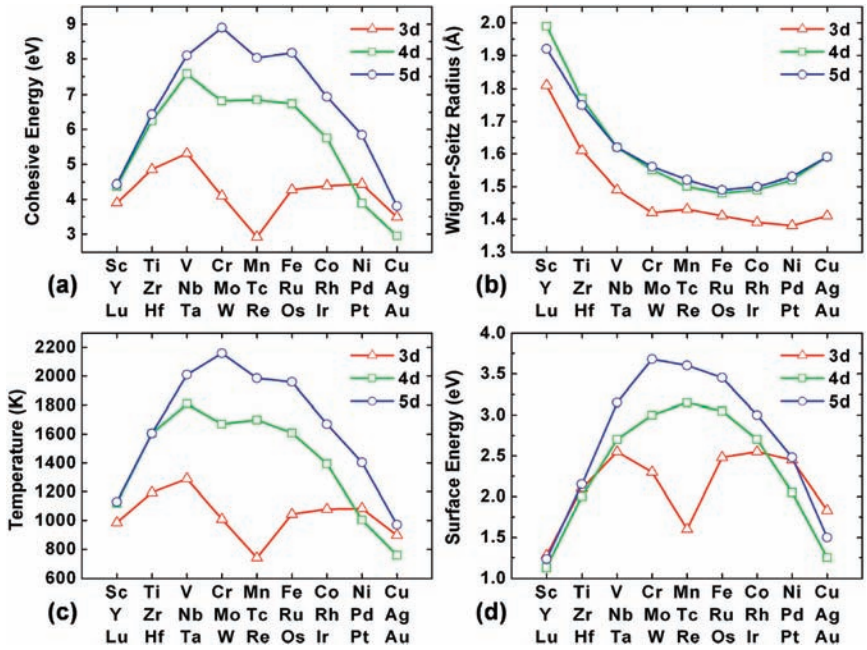

Figure 3. Properties of transition-metal series (a) cohesive energy (ref 28), (b) Wigner−Seitz radius (ref 28), (c) temperature at the vapor pressure of 10^{-10} Torr (ref 29), and (d) surface energy (ref 30).

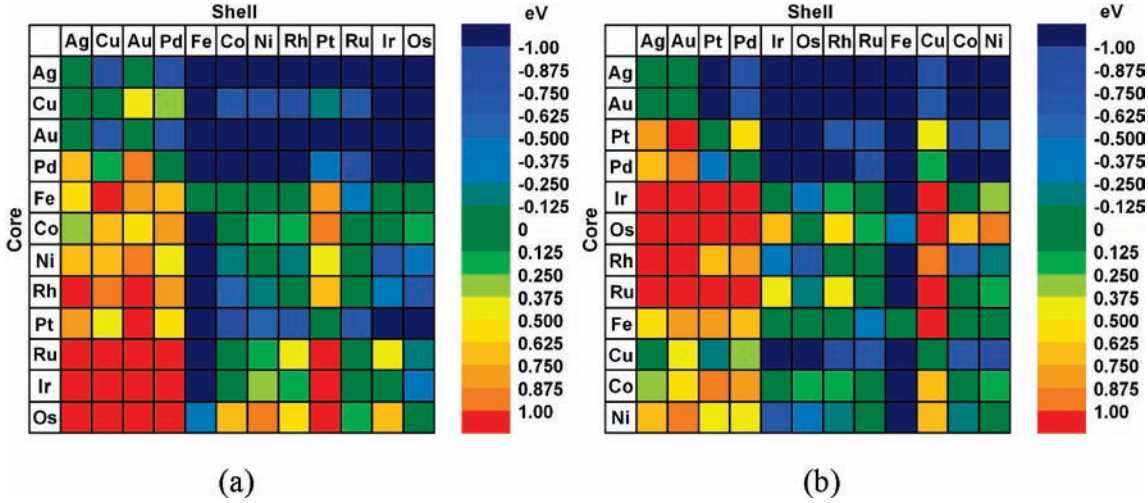

Figure 4. DFT-calculated SE (in *e*V) ordered in terms of (a) increasing cohesive energy and (b) decreasing WS radius. Color-coded matrix is as in Figure 2.

Such effects generally depend upon the relative difference in energy between the *d*-band center of the metallic system and the bonding molecular orbital level of the organic, as done for surfaces of metal and alloys by Norskov and co-workers,[39] or, more generally, for line compounds at all surface orientations by Wang and Johnson.[40]

For the future, we plan to determine the *d*-band centers for the alloyed nanoparticles and correlate these changes in the core−shell preference. However, simple correlations are already obvious from Figure 2. For example, a Ni-core/Pt-shell particle is a stable configuration and, given that they are in the same column of the periodic table, tight-binding arguments will have *d*-band centers near, but lower, than pure Pt, giving a favorable particle for oxidation−reduction reaction. (Indeed, such *d*-band effects dictate the formation enthalpy, thermodynamics and size effect in bulk NiPt.[31]) In addition, assessment of the temperature-dependent stability of the nanoparticles is needed, critical for use where, often, operational temperatures are at or above room temperature.

Universal Description of Core−Shell Preference. To provide insight into the general trends found for SE from the universal behavior of the electronic structure of core−shell nanoparticle, rather than trying to glean it from numerous ab initio calculations, we consider a generic *d*-band tight-binding model using the moment theorem[12−14] of density of states (DOS), successfully used in alloys for decades to explains bulk segregation[12] and ordering trends; and recently, similar analysis has been applied successfully to surface segregation.[5] According to the force theorem,[10−12] the energy change in a TM alloy due to a change in its configuration is, to first-order, the change in *d*-band energy, determined by *d*-bandwidth and filling. Assuming *d*-band filling of each metal is unchanged upon exchange of atoms, we can calculate band-energy difference and SE analytically.

(38) Hansen, P. L.; Wagner, J. B.; Helveg, S.; Rostrup-Nielsen, J. R.; Clausen, B. S.; Topsoe, H. *Science* **2002**, *295*, 2053–2055.
(39) Hammer, B.; Morikawa, Y.; Norskov, J. K. *Phys. Rev. Lett.* **1996**, *76*, 2141–2144.
(40) Wang, L. L.; Johnson, D. D. *J. Phys. Chem. C* **2008**, *112*, 8266–8275.

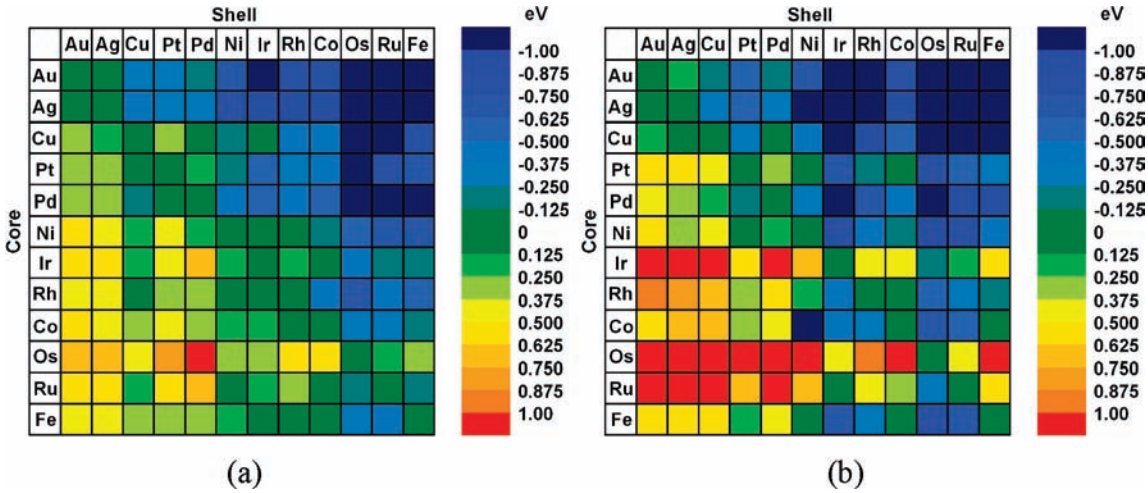

Figure 5. Calculated SE (in *e*V) for semi-infinite surfaces: (a) (111) (ref 5) and (b) (100) (ref 6). The data are color-coded and ordered in the same sequence as that in Figure 2 in terms of both cohesive energy (primary) and Wigner−Seitz radius (secondary).

At composition c_0, we find that the SE defined in eq 1 of exchanging one A in the core with one B in the shell (i.e., A from $c \rightarrow s$ and B from $s \rightarrow c$ with change in number $N_A^{c\rightarrow s} = N_B^{s\rightarrow c} = 1$) is a sum of the band-energy differences obtained from the first-moment of the DOS, i.e.,

$$\Delta E_{(A)B} = \Delta\mu_d^{A,c\rightarrow s}(c_0) + \Delta\mu_d^{B,s\rightarrow c}(c_0) \qquad (3)$$

Assuming a uniform distribution for *d*-band DOS (i.e., Friedel's model[41]) and arbitrary $N_A^{c\rightarrow s}$, the band-energy difference is obtained analytically as

$$\Delta\mu_d^{A,c\rightarrow s}(c_0) = 5\left[\left(\frac{n_d^A}{10}\right)^2 - \frac{n_d^A}{10}\right]\left\{6.83\left(\frac{\hbar^2}{m}\right)\frac{(r_d^A)^3}{(r_{WS})^5} \times \left[\sqrt{\frac{Z_s}{Z_b}} - \sqrt{\frac{Z_c}{Z_b}}\right]\right\}N_A^{c\rightarrow s} \qquad (4)$$

In eq 4, the change in *d*-bandwidth (in {.. .}) arises only from the first-shell coordination number $Z_{(c)s}$ [12 for core and 5 for shell] relative to bulk Z_b [12 for fcc]. Also, the WS radius is obtained as a composition-weighted average of the atomic volumes, i.e., $r_{WS}(c_0) = [c_0(r_{WS}^A)^3 + (1 - c_0)(r_{WS}^B)^3]^{1/3}$. All others quantities are known constants, such as number of *d*-electrons n_d^A in atom A and its effective radii r_d^A, which are specified, for example, in Harrison's solid-state table.[32] At the complementary composition of $(1 - c_0)$ with impurity atom of type B and the rest of type A, we change A $\leftrightarrow$ B and $c_0 \rightarrow (1 - c_0)$ in eqs 3 and 4 to get $\Delta E_{(B)A}$. Thus, the SE can be evaluated trivially within universal TB.

In Figure 6, we compare the SE evaluated from universal TB to that from our DFT-PW91 results (Table 1), where the coordination number in eq 4 was taken from the DFT calculations. Clearly, the SE from universal TB reproduces the DFT-PW91 results and trends very well. The TB results provide clear evidence that the origin of core−shell preference is *band-filling* and *bandwidth*, which are the only quantities included in eq 4 and which are manifested in the governing factors of *cohesive energy* and *average Wigner−Seitz radius*.

Our simple TB model does not include charge-transfer effects arising from electronegativity differences (i.e., band hybridization due to different *d*-band centers[42]). However, the model does determine the total cohesive energy of an alloyed nanoparticle mainly through its effects on the bandwidth and *d*-band energy due to changes in the average WS radius and coordination number. These two effects are enough to reproduce the trends in the DFT segregation energy. We note also that the cuboctahedral structure of Fe as host with a segregated impurity of other metal undergoes large structural relaxation that some of the (100) facets are distorted to be (111)-like, but the coordination number remains unchanged. In general, the band-energy difference in eq 4 due to distortion

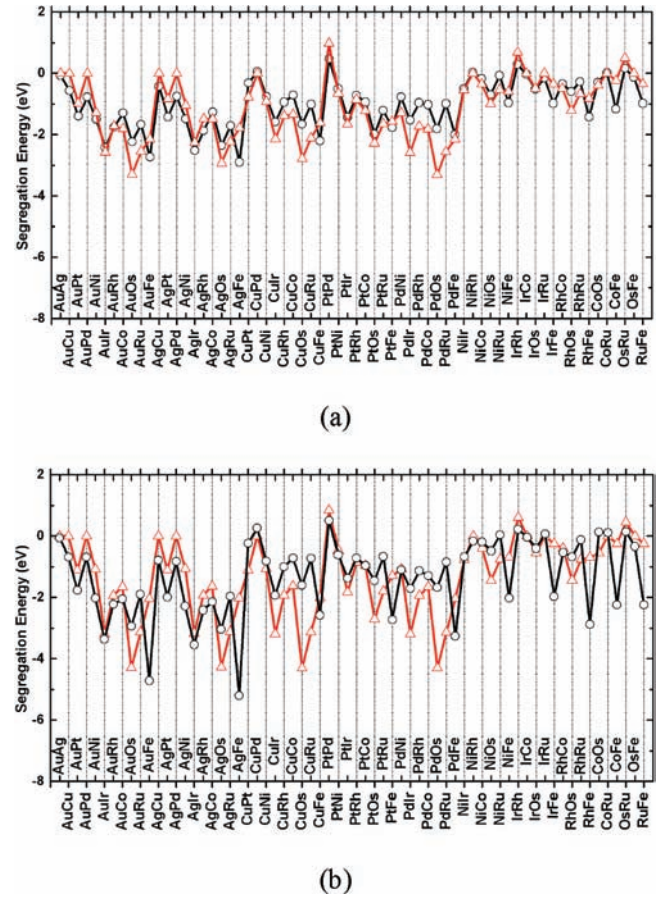

Figure 6. DFT-PW91 segregation energies (black circles) as listed and color-coded in Figure 2, compared to universal tight-binding band-energy differences (red triangles).

(41) Friedel, J. In *The Physics of Metals*; Ziman, J. M., Ed.; Cambridge University Press: New York, 1969, pp 494−525.
(42) Pettifor, D. G. *Phys. Rev. Lett.* **1979**, *42*, 846–850.

can be estimated by using the specific coordination numbers found in the DFT calculations.

Conclusions

Using the general concept of segregation energy (valid for bulk, semi-infinite bulk and nanoparticle alloys) calculated via ab initio density functional theory, we determined the core−shell preferences for 132 binary nanoparticle systems, composed of late transition-metals from groups 8−11 in the Periodic Table. Although it was a computational tour de force, we found, significantly, that the core−shell preferences from the segregation energies are described largely by only two independent key factors: (1) the *cohesive energy* and (2) the *Wigner−Seitz radius* (atomic size), and the interplay between them. For core−shell nanoparticles formed between atoms from different groups, the metal with the largest cohesive energy (the primary factor) goes into the core. For core−shell nanoparticles formed by atoms within a group, the metal with the smallest Wigner−Seitz radius (the secondary factor) determines core−shell preference, where the smallest atom goes into the core to relieve compressive strain; some exceptions exist for systems composed of 4d and 5d components, which are then dominated by cohesive energy, as the difference between the radii is too small. The same correlation is found for bulk and semi-infinite bulk alloy segregation energies. These findings serve as "design maps" that yield predictive guides to design alloyed nanoparticles. However, the core−shell preferences of the nanoparticles may be altered by molecular adsorbates/ligands, which depend on the relative placement of the bonding molecular level and the constituent d-band centroid, but may be predicted via similar methods. Finally, using the moment theorem in a tight-binding model to determine analytically the band-energy difference, we find that the segregation energies, arising from changes in cohesive energy (nearest-neighbor coordination number) and atomic size, reproduce the general trends found in the DFT segregation energies, providing confirmation as to the universal origin for core−shell preference in such nanoparticles.

Acknowledgment. Funding through the Department of Energy Catalysis (DEFG02-03ER15476) through the Frederick Seitz Materials Research Laboratory (DEFG02-91ER45439), Energy (DEFC36-05GO15064) with Sandia Metal-Hydride Center of Excellence, and BES (DEFG02-03ER46026) is gratefully acknowledged, along with thanks for the computational support from the Materials Computation Center (NSF DMR-0325939).

JA903247X